Chinese Journal of Mechanical Engineering

ORIGINAL ARTICLE

Open Access

High-Efficiency Dynamic Scanning Strategy for Powder Bed Fusion by Controlling Temperature Field of the Heat-Affected Zone

Xiaokang Huang[1], Xiaoyong Tian[1*], Qi Zhong[1], Shunwen He[1], Cunbao Huo[1], Yi Cao[1], Zhiqiang Tong[1] and Dichen Li[1]

Abstract

Improvement of fabrication efficiency and part performance was the main challenge for the large-scale powder bed fusion (PBF) process. In this study, a dynamic monitoring and feedback system of powder bed temperature field using an infrared thermal imager has been established and integrated into a four-laser PBF equipment with a working area of 2000 mm × 2000 mm. The heat-affected zone (HAZ) temperature field has been controlled by adjusting the scanning speed dynamically. Simultaneously, the relationship among spot size, HAZ temperature, and part performance has been established. The fluctuation of the HAZ temperature in four-laser scanning areas was decreased from 30.85 ℃ to 17.41 ℃. Thus, the consistency of the sintering performance of the produced large component has been improved. Based on the controllable temperature field, a dynamically adjusting strategy for laser spot size was proposed, by which the fabrication efficiency was improved up to 65.38%. The current research results were of great significance to the further industrial applications of large-scale PBF equipment.

Keywords Powder bed fusion, Efficiency, Large-scale, Spot size, Heat-affected zone (HAZ)

1 Introduction

Powder bed fusion (PBF) technology was one of the most popular rapid prototyping and manufacturing processes for complex parts with diverse material types [1–5], including metal [6], plastic [7], ceramic [8], etc., and is widely used in automotive, medical, military, aerospace and other fields [9–14]. Nowadays, a broad application of PBF in the industry was still limited [15] due to the relatively small effective building platform normally less than 1500 mm, and low fabrication efficiency. Thus, multi-laser powder bed fusion (MLPBF) has gradually gained attention in recent years and became one of the most promising technologies for the rapid manufacturing of large-scale parts [16–18].

MLPBF has enabled the PBF process to have a higher fabrication efficiency and a larger working area [17, 19–21]. An increment in building rate of 2.74 times (build time reduction of 63%) has been demonstrated in comparison to that of single-laser powder bed fusion (SLPBF) [22], but only within a working area of 250 mm × 250 mm. For the large-scale MLPBF process, EOS P 770 was a PBF machine with a two-laser system and an effective building volume of 700 × 380 × 580 mm^3. Huazhong University of Science and Technology, China, has successfully developed large-scale PBF equipment with a four-laser system [23] and an effective building volume of 1400 × 1400 × 500 mm^3. It was difficult for the MLPBF process to perform adequate quality evaluation and process optimization during large-scale part's sintering process [24]. In the synchronous scanning of multiple lasers, the difference

*Correspondence:
Xiaoyong Tian
leoxyt@mail.xjtu.edu.cn
[1] State Key Laboratory of Manufacturing Systems Engineering, Xi'an Jiaotong University, Xian 710049, China

in each laser's actual output power and the complex heat dissipation environment significantly impacted the sintering consistency among all laser scanning areas. Evaluating and optimizing multiple laser scanning fields' sintering consistency was of great significance to improving large-scale part's sintering quality. Many researchers tried to understand the relationship between the sintering temperature field and the process parameters in the sintering process [25–27]. However, it was only used for part's quality analysis after the sintering process and cannot provide effective help for optimizing the part quality in the sintering process.

Simultaneously, the small laser spot size is another limitation for the current MLPBF process to fabricate large-scale parts efficiently. More scholars have improved the production efficiency by expanding the spot size in the sintering process [28]. Bae and Kim [29, 30] designed a digital mirror system (DMS) that can deflect the laser beam with different spot sizes. This system can automatically expand the spot size 2× to 8×, and fabrication efficiency has been doubled. However, these researches lack the necessary experimental study on matching the spot size and process parameters.

Therefore, high-efficiency and high-quality stability have become the critical core issues of current large-scaled MLPBF equipment. In this study, a large-scale MLPBF equipment with a four-laser system has been established in the current research with an effective building volume of 2000 × 2000 × 1000 mm^3. A set of temperature field online monitoring and feedback system based on an infrared thermal imaging camera has been built and integrated into the MLPBF equipment, which can extract and analyze the temperature field in real-time during the sintering process. For a single laser scanning field, the relationship among spot size, scanning speed, sintering temperature, and part performance was established. The influence of spot size on the fabricating efficiency of parts has been further explored experimentally, and a dynamic scanning strategy with controllable spot size has been proposed in order to improve fabrication efficiency. For multiple laser scanning fields, an evaluation system for the consistency of sintering performance has been established through the differential analysis of temperature field data. The fluctuation of sintering temperature in each scanning field can be optimized by dynamically adjusting each laser scanning speed in the sintering process to improve the consistency of large-size part's sintering quality. Results in the current research will provide new ideas for the development of high-performance large-scale MLPBF equipment for industrial applications.

2 Materials and Methods

2.1 Four-laser PBF Equipment

As shown in Figure 1, a four-laser and four- galvanometer MLPBF equipment has been built, which can realize a build space of 2000 × 2000 × 1000 mm^3 through the cooperative control of four lasers. Four scanning galvanometers hurrySCAN® 30 were from SCANLAB company in Germany, and their effective maximum scanning speed can reach 5500 mm/s. Four CO_2 lasers (F200) were from American SYRAD of Novanta Inc., and their specific performance parameters were shown in Table 1. Four varioSCAN 40_{FLEX} were installed in the optical system as focusing systems on controlling the spot size from 1× to 5× dynamically.

In order to reduce the part's warpage in the sintering process, multilayer infrared heaters were installed to preheat the powder bed uniformly before laser sintering, as shown in Figure 1. An online monitoring and feedback system of the temperature field was also integrated into the MLPBF equipment based on the infrared thermal imager (FLIR A310) with a wide-angle lens, which can measure the overall temperature field in the working area of the powder bed during the laser sintering process, and the specific parameters of A310 are shown in Table 2.

2.2 Materials and Characterization

Resin-coated sand (German Huettenes-Albertus Chemwasche Werke Gmbh) was used as a raw material in the experiments, as shown in Table 3. Tensile tests of eight-shaped standard parts with a size of 35×66×12 mm were conducted referring to the Chinese Machinery Industry Standard GB/T 2684-2009 as shown in Figure 2, using a specialized testing machine (SWY, made by Changzhou Detu Precision Instrument Co., Ltd. of Jiangsu Province, China).

2.3 Experimental Plan

2.3.1 Fundamental Settings for Process Parameters

Improvement of fabrication efficiency can be achieved by changing the spot size. In this study, five-spot sizes magnified 1× to 5× were selected, and Figure 3(a) presents the scanning lines of different width made by five-spot sizes with a scanning speed of 2200 mm/s, and a laser power of 200 W. With the increase of spot size, their line width (L) was 2.1 mm, 3.8 mm, 6.1 mm, 7.2 mm, and 8.8 mm, respectively. As shown in Figure 3(b), the sintering layer in the two-dimensional plane comprises single scanning lines with specific spacing, and the spacing between adjacent scanning single lines was the hatch spacing (H). With the increase of L, the H can be appropriately increased to improve the fabrication efficiency.

In the PBF process, the interaction between laser and powder material was a thermal reaction process that

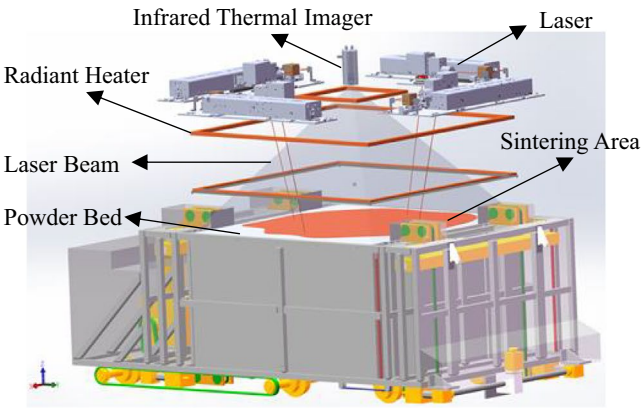

(a) Schematic diagram of large MLPBF equipment including four lasers and four scanning galvanometers

(b) Constructed MLPBF equipment

Figure 1 MLPBF equipment with a build space of 2000 × 2000 × 1000 mm^3

Table 1 Firestar laser F200 general specifications

Parameter	Value
Wavelength (μm)	10.2–10.7
Continuous maximum output power (W)	200
Peak maximum output power (W)	250

Table 2 The specific parameters of A310

Parameter	Value
Field angle (°)	90 × 73
Measuring temperature range (℃)	0–350 or 200–1200
Measurement frequency (Hz)	9
Resolution	320 × 240
Measurement accuracy (%)	± 2

needs to be detected and controlled to evaluate and optimize the part's quality. In this study, the HAZ temperature could be optimized by adjusting the laser scanning speed. Therefore, the relationship among laser scanning speed, laser spot, part performance, and HAZ temperature should be established in the sintering process, and the experimental parameters were shown in Table 4.

Table 3 The specific parameters of A310

Material properties	Value
Grain size (mm)	0.075–0.15
Melting point (℃)	88–94

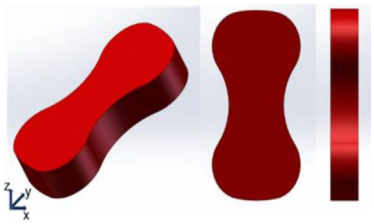

(a) Three-dimensional drawing of the eight-shaped standard part with 35×66×12 mm

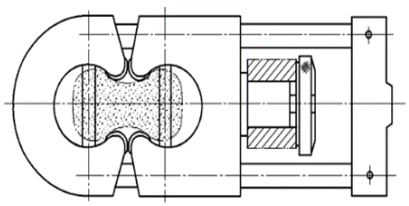

(b) Tensile strength test of "8" shaped standard parts

Figure 2 3D drawing and strength test of "8" shaped standard parts

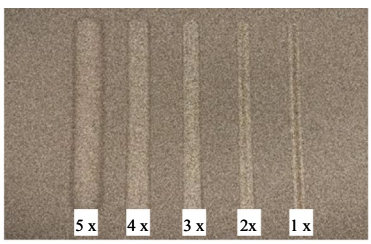

(a) The experimental results of the scanning line with different sizes of the laser spot

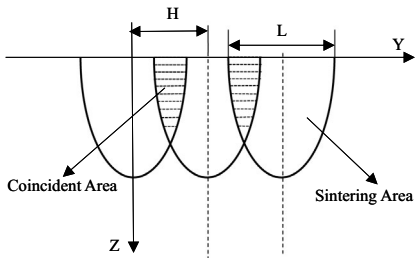

(b) Schematic diagram of hatch spacing

Figure 3 Influence of spot size on hatch spacing

2.3.2 Data Extraction of HAZ Temperature

The infrared thermal imager can monitor part's temperature field data in the fabricating process, and the average value of the HAZ temperature represented by T_s in each layer can be recorded. As shown in Figure 4(a), the infrared thermal imager can photograph the sintering process of the current sintering layer, and the temperature data in the sintering process can be processed and analyzed by the processing system. As shown in Figure 4(b), the whole fabricating process's temperature field data can be recorded in real-time, and the fabricating process of parts in each layer can be divided into three stages: preheating stage, sintering stage, and cooling stage. Each layer's sintering process's temperature field data contains two critical temperature characteristic values, namely T_{smax}, and T_m. T_{smax} represents the maximum value of T_s appears in the sintering stage, and T_m represents the average value of T_{smax} of all layers during part sintering, which can be calculated using the following equation:

Table 4 The specific parameters of A310

Parameter	Value
Laser power *P* (W)	200
Scanning speed *V* (mm/s)	Range from 1400–5000 at 200 intervals
Hatch spacing *H* (mm)	Range from 0.55–0.95 at 0.1 intervals
Magnification of laser spot *X*	Range from 1× to 5× at 1 intervals
Layer thickness *D* (mm)	0.30

(a) Temperature field data of the eight-shaped part in the fabricating process

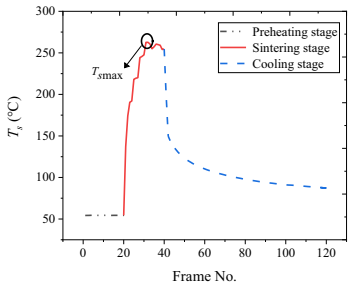

(b) Extraction of HAZ temperature data

Figure 4 The part's sintering process monitored by infrared thermal imager

$$T_m = \frac{\sum_{i=1}^{n} T_{s\max,i}}{n}, \quad (1)$$

$T_{s\max,i}$ was the maximum value of temperature in ith layer during the sintering process, n was the total number of layers. All characteristic values can be extracted by the online monitoring and feedback system of the temperature field based on the infrared thermal imager.

The real-time extraction of HAZ temperature data is of great significance to the optimization of the PBF process, and the relationships among spot size, process parameters, HAZ temperature, and part performance can be established on this basis. The HAZ temperature has an important influence on the part's strength, and within the reasonable range of HAZ temperature, the spot size can be dynamically changed for parts fabricating. Therefore, a high-efficiency scanning scheme based on dynamic spot size control could be established to achieve high fabrication efficiency.

2.3.3 High-Efficiency Scanning Process

The large-scale part can be divided into Skin region and Core region. The Skin region was sintered by using a small spot size to ensure the fabrication accuracy and strength, and the Core region was sintered by using a larger spot size to ensure fabrication efficiency.

As shown in Figure 5, the area with the height direction of 300–350 mm of the part is divided into skin and Core region s. The Skin region determines the final fabrication accuracy and strength of large-size parts. Therefore, It is necessary to improve the sintering consistency and the sintering strength in the four lasers' synchronous scanning process. Sintering performance is closely related to the HAZ temperature, which can be controlled by dynamically adjusting the scanning parameters. The Skin region can be divided into 20 sub-regions, and each laser scanning region covers 5 sub-regions. The strength of coated sand is characterized by measuring the tensile strength of eight-shaped standard parts, and an eight-shaped monitoring area is selected from each sub-region. When the scanning of each sub-region is completed in the current sintering layer, the temperature field data of HAZ in each sub-regions monitoring area can be extracted. After

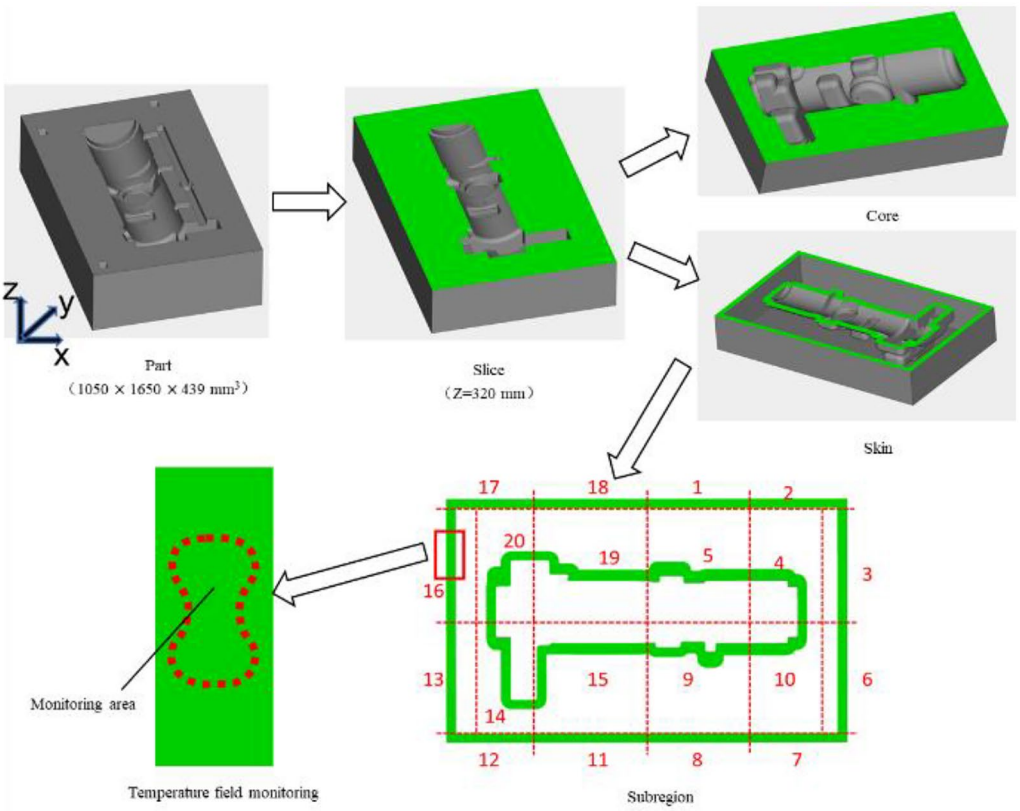

Figure 5 High-efficiency dynamic scanning strategy for large size parts by controlling HAZ temperature

analyzing each sub-regions temperature characteristic value, the processing system optimizes the sub-regions sintering strength by independently changing each sub-regions scanning speed in the next layer. Because the adjustment of the sub-regions scanning parameters is independent, and all sub-regions' target temperature is consistent. Therefore, the unity of four laser sintering performances can be optimized by reducing the difference of all sub-regions' HAZ temperatures in this way.

The Core region has a large building volume that determines the final fabrication efficiency of large-scale parts, and it has no strict requirements for sintering strength. Therefore, the Core region can be sintered by using a large spot size to improve fabrication efficiency. The relationship between spot size and fabricating efficiency can be determined by evaluating the effect of spot size on the HAZ temperature. On this basis, the optimal spot size can be selected to complete the Core region's fabricating.

3 Establishing the Relationships among Spot Size, Process Parameters, HAZ Temperature, and Part Performance

The relationship between spot size and fabrication efficiency needs to be explored to complete the large-scale part's high-efficiency scanning process. The appropriate spot size for the Skin region and Core region of large-scale parts can be selected on this basis. At the same time, the relationship among process parameters, HAZ temperature, and part performance should also be confirmed to optimize the Skin's sintering strength and the consistency of the four lasers' synchronous scanning quality.

3.1 Influence of Scanning Speed and Spot Size on HAZ Temperature

The spot size can be magnified from 1× to 5× using dynamic focusing systems with a consistent laser power of 200 W, and the relationship between scanning speed and HAZ temperature of the parts under different spot sizes has been explored. The experimental results were shown in Figure 6. It can be found that the HAZ temperature of the parts gradually decreases with the increase of scanning speed and spot size due to the decreasing laser power density. The temperature field data have been numerically fitted, and the relevant results were shown in Table 5. It can be found that the HAZ temperature and the scanning speed of the parts present an exponential relationship.

Figure 7 shows that the HAZ temperature has an important influence on part's sintering quality. When the HAZ temperature was too low, the corresponding T_m was lower than 230 ℃, which resulted in the collapse of the part because of the insufficient laser energy. When the HAZ temperature was too high, the corresponding T_m was greater than 270 ℃, which resulted in a significant part's over-burning due to the excess laser energy.

Table 5 Equation relationship between scanning speed and T_m

Magnification of spot size	Fitting equation
1×	$T_m = 110.9e^{\frac{-V}{2936}} + 209.1$
2×	$T_m = 109.7e^{\frac{-V}{2345}} + 212.0$
3×	$T_m = 108.8e^{\frac{-V}{3173}} + 196.3$
4×	$T_m = 117.7e^{\frac{-V}{3997}} + 180.7$
5×	$T_m = 102.3e^{\frac{-V}{3765}} + 181.3$

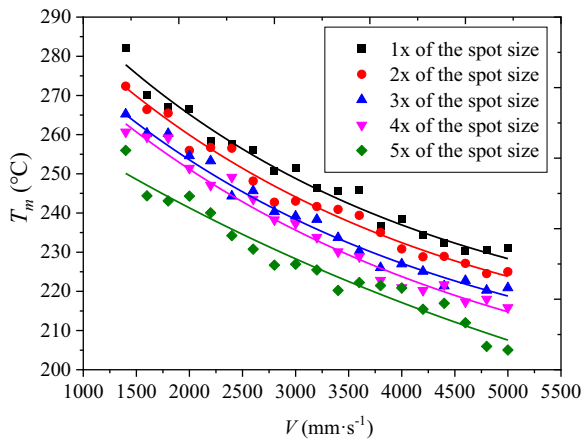

Figure 6 Correlation diagram of scanning speed V and T_m with different spot sizes

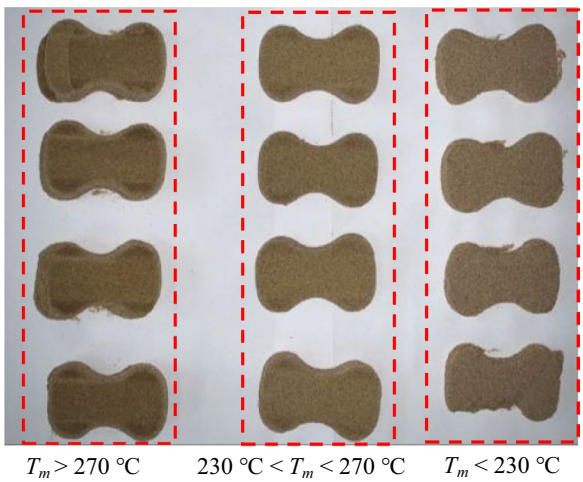

Figure 7 Fabricated eight-shaped parts under different HAZ temperature

Therefore, a reasonable T_m value from 230 to 270 ℃ was required to achieve a better part quality during the sintering process.

3.2 Influence of HAZ Temperature on the Properties of Parts

Experimental results have shown that improper HAZ temperature was an important reason for the part's defects, and the HAZ temperature of the parts must be controlled between 230 ℃ and 270 ℃. A total of five temperature range were selected, which were 268 ± 2 ℃, 260 ± 2 ℃, 252 ± 2 ℃, 244 ± 2 ℃, 236 ± 2 ℃. According to the experimental results of Figure 6, the spot size and scanning parameters can be determined corresponding to each temperature range.

The strength test of the parts in these five temperature ranges has been carried out, and the experimental results were shown in Figure 8. The experimental results show that the part's tensile strength fluctuates slightly when the HAZ temperature remains stable. The tensile strength of the parts increases with the increase of the HAZ temperature.

For the part's Skin region, the smallest spot size must be used to ensure the large-size part's fabricating accuracy and strength. Figure 9 shows the maximum scanning speed for each temperature range when the spot size is magnified by 1×. Figures 8 and 9 shows that when the HAZ temperature of the part rises from 258 ℃ to 267 ℃, The strength of the part is increased by 6.9%, while the scanning speed reduced by 18.2%. Therefore, 258 ℃ can be set as the best T_m value to ensure that the parts have high strength with specific fabrication efficiency.

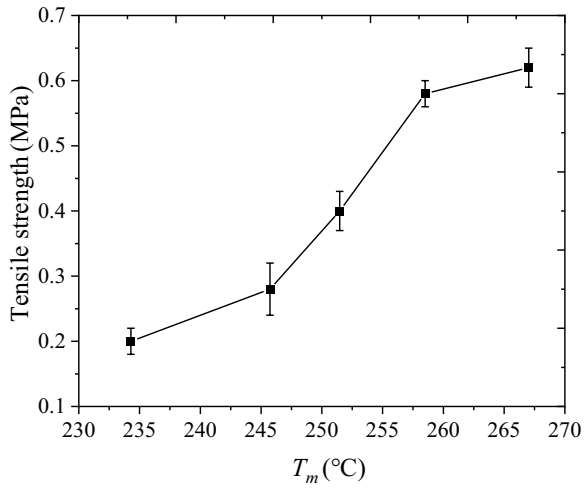

Figure 8 Correlation diagram between the tensile strength of the part and T_m

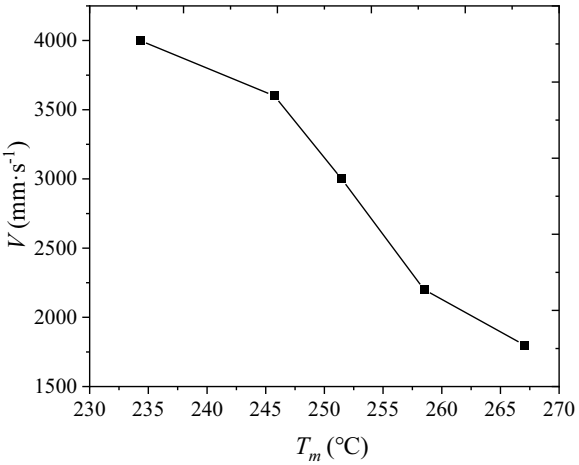

Figure 9 Correlation diagram between the tensile strength of the part and Temperature range

According to different fabricating targets, there were two fabricating modes to select. The first was the performance priority mode. In this mode, the part's sintering temperature was set to 258 ℃, and the fabricated parts could have high strength with general efficiency. The second mode was the efficiency priority mode, in which the part's sintering temperature was set to 234 ℃, and the parts could have higher production efficiency with general mechanical strength. For the large-scale parts, the performance priority mode can be selected in the Skin region to ensure the fabricating strength of large-scale parts, and the efficiency priority mode can be selected in the Core region to improve the fabrication efficiency of large-scale parts. Finally, the high-efficiency and high-performance fabricating of large-scale parts can be realized through two fabricating modes' collaboration.

3.3 Influence of Spot Size on Fabrication Efficiency

For the PBF process, scanning speed V and hatch spacing H were essential factors that affect the part's fabrication efficiency. Therefore, the efficiency factor M can be introduced to describe the part's fabrication efficiency with different process parameters. Its expression was as follows:

$$M=VD. \tag{2}$$

It can characterize the scanning area in unit time during the sintering process. The maximum fabrication efficiency of each spot size represented by $M_{\max}$ can be calculated by Eq. (2) and Figure 6 under the efficiency priority mode. The calculation results were shown in Figure 10. Initially, the $M_{\max}$ increases with the increase of spot size and then decreases. Because the spot size increases, process parameters must be adjusted

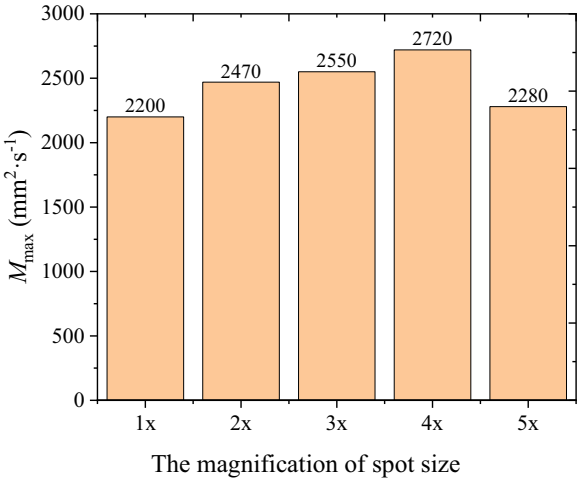

Figure 10 The value of M_{max} with different spot sizes.

accordingly. While the laser power was limited to 200 W, and the value of hatch spacing was related to the spot size, to ensure that parts can be fabricated, the scanning speed must be reduced to ensure enough sintering energy that makes parts can be fabricated, which leads to the decrease of M_{max}. Therefore, it was necessary to select the appropriate spot size to ensure fabrication efficiency. At the same time, Figure 10 shows that the fabrication efficiency can reach the maximum value when the spot size was magnified by 4×. The corresponding process parameters were laser power of 200 W, hatch spacing of 0.85 mm, and scanning speed of 3200 mm/s.

4 High-Efficiency Laser Sintering Strategy

4.1 Dynamic Control of HAZ Temperature

The relationship between scanning speed and HAZ temperature has been established experimentally. The equation relationship between the adjustment value of the temperature field and the adjustment value of scanning speed can be found, which can be expressed in terms of Eq. (3):

$$\begin{cases} T_m = F(V), \\ \Delta V = \Delta T_m \dfrac{\partial F^{-1}(T_m)}{\partial T_m}, \end{cases} \tag{3}$$

ΔT_m is the temperature adjustment value, and ΔV is the scanning speed adjustment value. As shown in Figure 11, the Skin region's HAZ temperature can be controlled by the control logic. The T_{smax} values of the current layer in all monitoring areas can be measured using the infrared thermal imager during the sintering process. The deviation between the T_{smax} and the target temperature (258 ℃) can be calculated in each subregion. The adjusted values ΔV for each sub-region's laser scanning speed

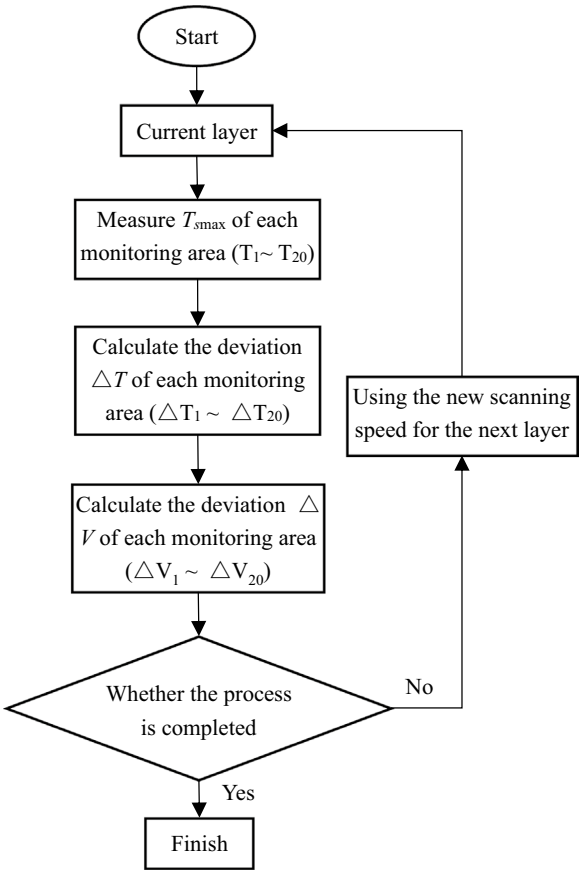

Figure 11 Control strategy of HAZ temperature

can be calculated as ΔV_1, ΔV_2, ..., and ΔV_{20} by Eq. (3) and Table 4, which will be passed as a feedback signal to the equipment process system. Finally, each sub-region's laser scanning speed was adjusted and applied to the next layer's sintering process. This cycle will be continued until part sintering was completed.

4.2 Experimental Verification

The infrared thermal imager can record the part's temperature field data during the sintering process. As shown in Figure 12, all monitoring areas' sintering temperature

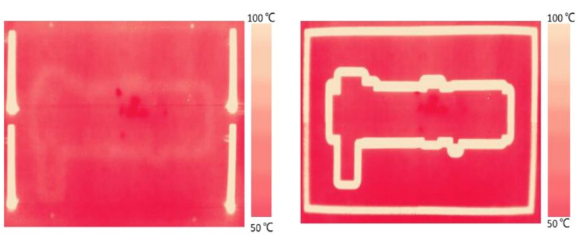

Figure 12 Picture of temperature field during the sintering process of large-sized part captured by an infrared thermal imager

field data can be extracted during the sintering process. The sintering quality of parts can be evaluated by analyzing all sintering layers' temperature field data, and then different process strategies can be compared.

A monitoring area was selected in each laser scanning area. Then their temperature fields were compared and analyzed using different process strategies, and the experimental results were shown in Figure 13.

Since the HAZ temperature adjustment process requires a stable stage, the first few layers' temperature fields were unstable, so the calculation and analysis were started from the fifth layer. For the monitoring areas' temperature field data distributed in the subregion 1 of laser 1 scanning region, the fluctuation of all sintering layers' sintering temperature is large when using constant process parameters, and the whole fluctuation range from 234.8 ℃ to 276.6 ℃. The fluctuation of all sintering temperature fields is significantly reduced when using regulatable process parameters, and the whole fluctuation range from 249.8 ℃ to 269.7 ℃, which decreases by 48.66%. It can be proved that using regulatable process parameters can more effectively make the HAZ temperature closer to the target temperature, which can improve the sintering strength of the part's Skin region.

Furthermore, it can be found that the HAZ temperature presents an upward trend in the whole fabricating process when using constant process parameters. The reason was that the part's sintering temperature was affected by the heat accumulation during the sintering process and the gradually rising ambient temperature of the powder bed with the extension of fabricating time, which affects the sintering's overall uniformity temperature field. This defect can be virtually eliminated when using regulatable process parameters.

4.3 Discussion

4.3.1 Consistency Evaluation of Sintering Quality

Figure 14 shows the fluctuation in the T_{smax} range in 20 monitoring areas using two process strategies. The uniformity of the HAZ temperature improved gradually with the increase in the sintering layer number. Finally, compared with using constant process parameters, the average temperature field range of 20 monitoring areas was reduced from 30.85 ℃ to 17.41 ℃ when using regulatable process parameters. This is because the four lasers' real spot size and output power are different. Therefore, the HAZ temperature in the four scanning areas is quite different. The variability of the HAZ temperature in the four scanning areas can be effectively reduced by independently adjusting the four lasers' scanning speed and then effectively improving the consistency of the sintering performance of large-size parts

Thermogravimetric (TG) experiments were performed on the materials in four laser scanning areas of the parts fabricated using the two different scanning strategies, as shown in Figure 15. TG's value can reflect the resin's residual quality in the sintered coated sand, and it can indirectly reflect the sintering degree of the coated sand. The experimental results show that the TG difference range of the four laser scanning regions decreases from 0.4242% to 0.1589%, which decreases by 62.5%. Therefore, it could prove that the uniformity of the sintering degree of the four laser scanning areas of the part had been effectively improved when using regulatable process parameters.

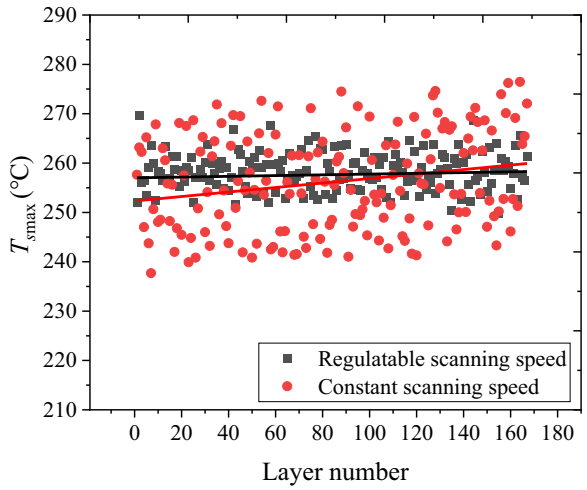

Figure 13 HAZ temperature fluctuations of subregion 1 in laser 1 scanning region

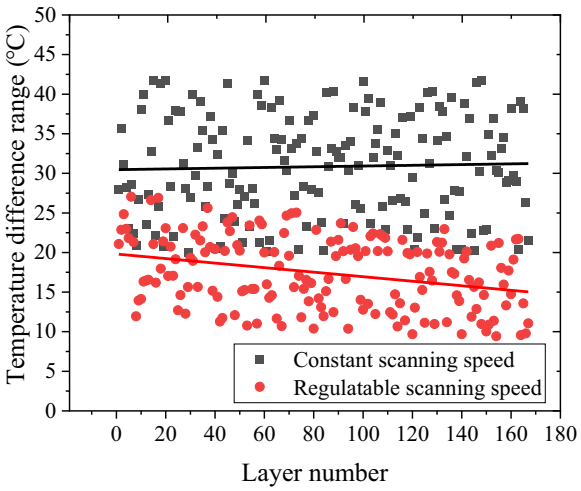

Figure 14 The fluctuation of T_{smax} range value in 20 monitoring areas with two process strategies

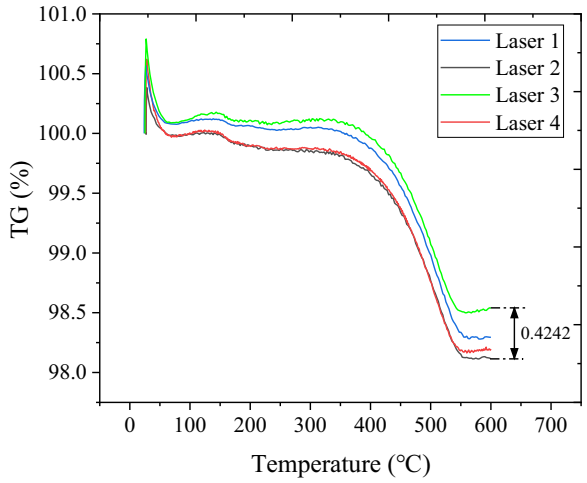

(a) Constant scanning speed

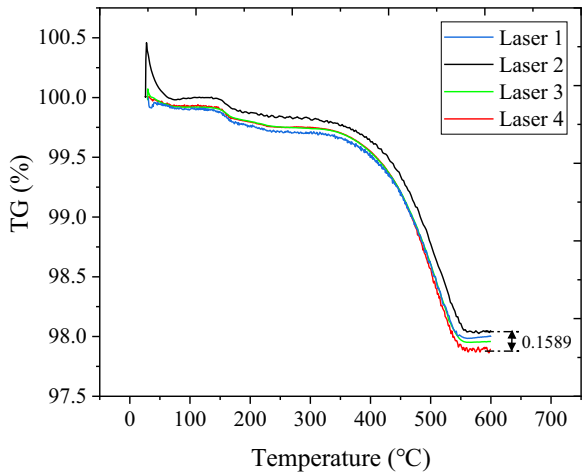

(b) Regulatablet scanning speed

Figure 15 Result of the thermogravimetric experiment

4.3.2 Fabrication Efficiency Evaluation

The high-efficiency scanning process has been used to print the upper mold and the bottom mold, compared with a controlled experiment that uses the fixed spot size. The upper mound with a size of 1650 × 1050 × 311 mm^3 and the bottom mold with a size of 1650 × 1050 × 439 mm^3 have been fabricated as shown in Figure 16.

The high-efficiency scanning scheme based on dynamic spot size control aims to improve the fabrication efficiency of the PBF process. Therefore, the fabricating time was an important criterion [31]. As shown in Table 6, compared with a controlled experiment that was using the fixed laser spot process, experimental results by using a high-efficiency PBF process based on

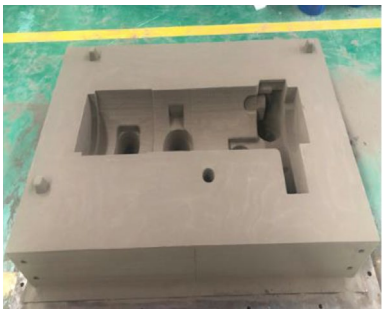

(a) The upper mold with a size of 1650 × 1050 × 311 mm

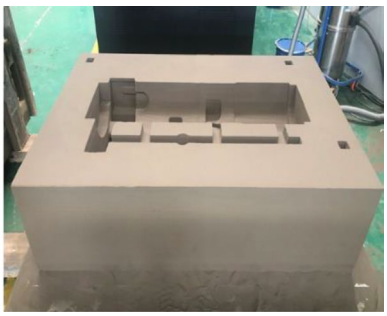

(b) The bottom mold with a size of 1650 × 1050 × 439 mm

Figure 16 Large-scale parts fabricated by MLPBF equipment

variable laser spot show that the fabrication efficiency of the upper mold was increased by 57.54% and that of the bottom mold was increased by 65.38%.

5 Conclusions

In this study, a temperature-field monitoring system has been established in a four-laser MLPBF equipment based on an infrared thermal imager. The HAZ temperature of large-scale parts during the sintering process was dynamically controlled by adjusting the scanning speed of four lasers independently, and the difference in sintering performance of four laser scanning areas has been reduced. Simultaneously, the influence of the HAZ temperature on the tensile strength of parts has been explored. The relationship between spot size and the fabrication efficiency of parts has been established. Finally, a high-efficiency scanning process scheme based on dynamic spot size

Table 6 Fabricated time of upper mold and the bottom mold with different PBF process

PBF process	Build-time of upper mold (h)	Build-time of bottom mold (h)
Fixed laser spot process	145.9	194.1
Variable laser spot process	92.61	117.6

control has been proposed, and the PBF fabrication efficiency of large size parts has been significantly improved.

Acknowledgments
Not applicable.

Authors' Contributions
XYT developed the idea and revised the paper. XKH developed the idea, designed and performed the experiments, analyzed data, and wrote the paper. Other authors participated in the discussion of the experiment and the revision of the paper. All authors read and approved the final manuscript.

Funding
Supported by National High Technology Research and Development Program of China (863 Program, Grant No. 2015AA042503), and K. C. Wong Education Foundation.

Availability of Data and Materials
Not applicable.

Declarations

Competing Interests
The authors declare no competing financial interests.

Received: 28 June 2021 Revised: 30 November 2021 Accepted: 12 January 2024
Published online: 11 March 2024

References

[1] Z Sajedi, R Casati, M C Poletti, et al. Thermal fatigue testing of laser powder bed fusion (l-pbf) processed alsi7mg alloy in presence of a quasi-static tensile load. *Materials Science and Engineering: A*, 2020, 789: 139617.
[2] C Chen, Z Xiao, H Zhu, et al. Distribution and evolution of thermal stress during multi-laser powder bed fusion of ti-6al-4 v alloy. *Journal of Materials Processing Technology*, 2020, 284: 116726.
[3] M Strantza, R K Ganeriwala, B Clausen, et al. Effect of the scanning strategy on the formation of residual stresses in additively manufactured ti-6al-4v. *Additive Manufacturing*, 2021, 45: 102003.
[4] L Scime, J Beuth. Using machine learning to identify in-situ melt pool signatures indicative of flaw formation in a laser powder bed fusion additive manufacturing process. *Additive Manufacturing*, 2019, 25: 151-165.
[5] E Santecchia, P Mengucci, A Gatto, et al. Laser powder bed fusion: tailoring the microstructure of alloys for biomedical applications. *Materials Today-Proceedings*, 2019, 19(SI1): 24-32.
[6] X Zhao, S Li, M Zhang, et al. Comparison of the microstructures and mechanical properties of ti–6al–4v fabricated by selective laser melting and electron beam melting. *Materials & Design*, 2016, 95: 21-31.
[7] J Liu, C Gao, P Feng, et al. Selective laser sintering of β-tcp/nano-58s composite scaffolds with improved mechanical properties. *Materials & Design*, 2015, 84: 395-401.
[8] C Shuai, C Gao, Y Nie, et al. Structural design and experimental analysis of a selective laser sintering system with nano-hydroxyapatite powder. *Journal of Biomedical Nanotechnology*, 2010, 6(4): 370-374.
[9] A Enzi, J A Mynderse. Design and experimental validation of a small-scale prototype selective laser sintering system. *Sn Applied Sciences*, 2019, 1(12): 1612.
[10] M X Yan, X Y Tian, D C Li. Powder bed fusion of the polyaryletherketone and composites with high performance-research status and challenge. *Journal of Netshape Forming Engineering*, 2019, 11(04): 64-72.
[11] M Q Xia. Optimization of engine cylinder by additive manufacturing technology. *Ordnance Material Science and Engineering*, 2020, 43(06): 25.
[12] L Lu. Additive manufacturig applied in aviatic casting. *Materials Reports*, 2018, 32(S1): 390-394.
[13] X W Zhang. Application of metal additive manufacturing in aero-engine. *Journal of Aerospace Poer*, 2016, 31(01): 10-16.
[14] T Pan, W Zhu, C Z Yan, et al. Selective laser sintering 3D printing of biomedical polymer materials. *Polymer Materials Science and Engineering*, 2016, 32(03): 178-183.
[15] M Schmidt, M Merklein, D Bourell, et al. Laser based additive manufacturing in industry and academia. *CIRP Annals-Manufacturing Technology*, 2017, 66(2): 561-583.
[16] L Cao. Numerical investigation on molten pool dynamics during multi-laser array powder bed fusion process. *Metallurgical and Materials Transactions A-Physical Metallurgy and Materials Science*, 2021, 52(1): 211-227.
[17] P Wagenblast, J Risse, S Schweikert, et al. Multi-laser fusion process with pre-heating for additive Manufacturing. In: B Gu, H Chen, H Helvajian. *Proceedings of SPIE*, 2020.
[18] F Eibl, C Tenbrock, T Pichler, et al. Alternative beam sources and machine concepts for laser powder bed fusion. *High Power Diode Lasers and Systems Conference*, 2017: 7-8.
[19] S Li, J Yang, Z Wang. Multi-laser powder bed fusion of Ti-6.5Al-2Zr-Mo-V alloy powder: Defect formation mechanism and microstructural evolution. *Powder Technology*, 2021, 384: 100-111.
[20] K Wei, F Li, G Huang, et al. Multi-laser powder bed fusion of Ti-6Al-4V alloy: Defect, microstructure, and mechanical property of overlap region. *Materials Science and Engineering A-Structural Materials Properties Microstructure and Processing*, 2021, 802: 140644.
[21] F Li, Z Wang, X Zeng. Microstructures and mechanical properties of Ti6Al4V alloy fabricated by multi-laser beam selective laser melting. *Materials Letters*, 2017, 199: 79-83.
[22] H Wong, K Dawson, G A Ravi, et al. Multi-laser powder bed fusion benchmarking-initial trials with inconel 625. *International Journal of Advanced Manufacturing Technology*, 2019.
[23] S F Wen, C Z Yan, Q S Wei, et al. Investigation and development of large-scale equipment and high performance materials for powder bed laser fusion additive manufacturing. *Virtual and Physical Prototyping*, 2014, 9(4): 213-223.
[24] M Grasso, B M Colosimo. Process defects and in situ monitoring methods in metal powder bed fusion: A review. *Measurement Science and Technology*, 2017, 28: 0440054.
[25] H Kim, Y Lin, T B Tseng. A review on quality control in additive manufacturing. *Rapid Prototyping Journal*, 2018, 24(3SI): 645-669.
[26] W W Wroe, J Gladstone, T Phillips, et al. In-situ thermal image correlation with mechanical properties of nylon-12 in SLS. *Rapid Prototyping Journal*, 2016, 22(5SI): 794-800.
[27] M Abdelrahman, T L Starr. Quality certification and control of polymer laser sintering: layerwise temperature monitoring using thermal imaging. *International Journal of Advanced Manufacturing Technology*, 2016, 84(5-8): 831-842.
[28] D Miller, C Deckard, J Williams. Variable beam size sls workstation and enhanced SLS model. *Rapid Prototyping Journal*, 1997, 3(1): 4-11.
[29] S W Bae, J S Kim, D S Kim, et al. An experimental study for rising manufacturing time and accuracy on SLS process. *2009 IEEE International Symposium on Assembly and Manufacturing*, 2009: 83-87.
[30] D S Kim, S W Bae, K H Choi. Application and performance evaluation for the DMS system in the SLS process. *International Journal of Modern Physics B*, 2008, 22(9-11): 1833-1838.
[31] C Yi, L Dichen, W Jing. Using variable beam spot scanning to improve the efficiency of stereolithography process. *Rapid Prototyping Journal*, 2013, 19(2): 100-110.

Xiaokang Huang (1991.07), male, Xi'an City, Shaanxi Province, China. Ph.D. candidate, *State Key Laboratory for Manufacturing System Engineering, Xi'an Jiaotong University*, *China*. His research topic is the high efficiency and high precision process of large-scale powder bed fusion equipment.

Xiaoyong Tian (1981.07), male, Xi'an City, Shaanxi Province, China. Ph.D. Professor, *State Key Lab for Manufacturing System Engineering in Xi'an Jiaotong University, China*. His research field is additive manufacturing (AM) of advanced composite materials.

Qi Zhong (1993.06), male, Xi'an City, Shaanxi Province, China, Ph.D. candidate, *State Key Laboratory for Manufacturing System Engineering, Xi'an Jiaotong University, China*. His research topic is the intelligent monitoring and digital manufacturing of powder bed fusion.

Shunwen He (1992.07), male, Xi'an City, Shaanxi Province, China. M.D. graduated from *Xi'an Jiaotong University, China*. His research direction is to optimize the powder bed fusion process based on temperature field control.

Cunbao Huo (1994.07), male, Xi'an City, Shaanxi Province, China. Ph.D. candidate, *State Key Laboratory for Manufacturing System Engineering, Xi'an Jiaotong University, China*. His research is focusing on 3D printing of functional structural ceramics.

Yi Cao (1983.06), male, Xi'an City, Shaanxi Province, China. Ph.D. Senior engineer, State Key Laboratory for Manufacturing System Engineering, Graduated from *Xi'an Jiaotong University, China*. His research direction is the additive manufacturing of polymers.

Zhiqiang Tong (1985.05), male, Xi'an City, Shaanxi Province, China. Engineer, *State Key Laboratory for Manufacturing System Engineering, Xi'an Jiaotong University, China*. His research topic is 3D printing of high-performance metal material.

Dichen Li (1964.07), male, Xi'an City, Shaanxi Province, China. Ph.D. Professor, Director of *State Key Lab for Manufacturing System Engineering in Xi'an Jiaotong University, China*. His research fields include additive manufacturing(AM), bio-fabrication, and shaping of composite materials.